



**HAL**  
open science

## Observation of water vapor in the stratosphere of Jupiter with the Odin Space Telescope.

T. Cavalié, F. Billebaud, N. Biver, M. Dobrijevic, E. Lellouch, J. Brillet, J.  
Lecacheux, A. Hjalmarson, A. Sandqvist, U. Frisk, et al.

► **To cite this version:**

T. Cavalié, F. Billebaud, N. Biver, M. Dobrijevic, E. Lellouch, et al.. Observation of water vapor in the stratosphere of Jupiter with the Odin Space Telescope.. Planetary and Space Science, 2008, 56 (12), pp.1573-1584. 10.1016/j.pss.2008.04.013 . hal-00261908

**HAL Id: hal-00261908**

**<https://hal.science/hal-00261908v1>**

Submitted on 10 Mar 2008

**HAL** is a multi-disciplinary open access archive for the deposit and dissemination of scientific research documents, whether they are published or not. The documents may come from teaching and research institutions in France or abroad, or from public or private research centers.

L'archive ouverte pluridisciplinaire **HAL**, est destinée au dépôt et à la diffusion de documents scientifiques de niveau recherche, publiés ou non, émanant des établissements d'enseignement et de recherche français ou étrangers, des laboratoires publics ou privés.

# Observation of water vapor in the stratosphere of Jupiter with the Odin Space Telescope

T. Cavalié<sup>a,\*</sup>, F. Billebaud<sup>a</sup>, N. Biver<sup>b</sup>, M. Dobrijevic<sup>a</sup>,  
E. Lellouch<sup>b</sup>, J. Brillet<sup>a</sup>, A. Lecacheux<sup>b</sup>, Å. Hjalmarson<sup>c</sup>,  
Aa. Sandqvist<sup>d</sup>, U. Frisk<sup>e</sup>, M. Olberg<sup>c</sup>, The Odin Team,  
E.A. Bergin<sup>f</sup>

<sup>a</sup>*Université Bordeaux 1; CNRS; OASU; LAB, UMR 5804, 331270 Floirac, France*

<sup>b</sup>*LESIA, Observatoire de Paris, 92195 Meudon, France*

<sup>c</sup>*Onsala Space Observatory, 43992 Onsala, Sweden*

<sup>d</sup>*Stockholm Observatory, 10691 Stockholm, Sweden*

<sup>e</sup>*Swedish Space Corporation, 17104 Solna, Sweden*

<sup>f</sup>*Harvard-Smithsonian Center for Astrophysics, Cambridge MA 02138, USA*

---

## Abstract

The water vapor line at 557 GHz has been observed with the Odin space telescope with a high signal-to-noise ratio and a high spectral resolution on November 8, 2002. The analysis of this observation as well as a re-analysis of previously published observations obtained with the Submillimeter Wavelength Astronomy Satellite seem to favor a cometary origin (Shoemaker-Levy 9) for water in the stratosphere of Jupiter, in agreement with the ISO observation results. Our model predicts that the water line should become fainter and broader from 2007. The observation of such a temporal variability would be contradictory with an IDP steady flux, thus

supporting the SL9 source hypothesis.

*Key words:* Jupiter, atmosphere, water, spectroscopy, Odin space telescope

---

## 1 Introduction

2 The Infrared Space Observatory has detected water vapor in the stratospheres  
3 of the giant planets (Feuchtgruber et al. 1997; Feuchtgruber et al. 1999; Lel-  
4 louch 1999). The large amount of water measured above the condensation  
5 level of vapor (cold trap at the tropopause) implies the presence of an ex-  
6 ternal source of oxygenated compounds (Moses et al. 2000b; Lellouch et al.  
7 2002). These compounds could be brought by interplanetary dust particles  
8 (IDP), sputtering from the rings and/or satellites and large cometary im-  
9 pacts. Observations of Jupiter carried out by ISO tend to prove that most of  
10 the stratospheric water is due to the Shoemaker-Levy 9 (SL9) comet impacts  
11 in July 1994 (Lellouch et al. 2002), whereas Bergin et al. (2000) obtained sat-  
12 isfactory fits to the Submillimeter Wavelength Astronomy Satellite (SWAS)  
13 data by considering IDP infall, with a constant flux of  $2.0 \times 10^6 \text{ cm}^{-2} \cdot \text{s}^{-1}$ .

14 The submillimeter satellite Odin was launched in 2001 and obtained a high  
15 resolution spectrum of Jupiter's water vapor line ( $1_{10}-1_{01}$ ) at 557 GHz on  
16 November 8, 2002. This spectrum is presented in this work as well as a re-  
17 analysis of SWAS observations. Spectral analysis combined with the use of our  
18 photochemical model (Ollivier et al. 2000, adapted to Jupiter) provides new  
19 clues which help understanding the origin of water vapor in the stratosphere

---

\* Tel: +33-5-5777-6123; fax: +33-5-5777-6110

*Email address:* Thibault.Cavalié@obs.u-bordeaux1.fr (T. Cavalié).

20 of Jupiter.

21 A description of the observations is given in Sect. 2. Our photochemical and  
22 radiative transfer models are described in Sect. 3. Our results are presented  
23 in Sect. 4 and the different sources of H<sub>2</sub>O are discussed in Sect. 5.

## 24 **2 Observations**

25 The space telescopes SWAS and Odin observed the water vapor 557 GHz line  
26 on Jupiter in 1999, 2001 (SWAS) and 2002 (Odin). The resulting brightness  
27 temperature spectra have a signal-to-noise ratios of  $\sim 17$ , 10 and 16 respec-  
28 tively for the 1999, 2001 and 2002 observations. The spectral resolution is  
29 about  $1 \text{ km.s}^{-1}$  for the SWAS spectra and  $0.6 \text{ km.s}^{-1}$  for the Odin spectrum.

30 The SWAS spectra are corrected for the Double Side Band (DSB) response  
31 of the instrument. Nevertheless, the SWAS spectra show broad features at  
32  $100 \text{ km.s}^{-1}$  and more, which cannot be reproduced in models. These wings,  
33 probably due to instrumental effects as mentionned in Bergin et al. (2000)  
34 and Lellouch et al. (2002), cause an uncertainty on the continuum level of the  
35 emission. More details on the SWAS 1999 and 2001 observations can be found  
36 in Bergin et al. (2000) and Lellouch et al. (2002).

37 The Odin observations were carried out with the Acousto-Optical Spectrome-  
38 ter (AOS) in a classical position switching mode (Olberg et al. 2003). The re-  
39 ceivers are operated in a Single Side Band (SSB) mode. The spectral band is 1  
40 GHz. As Jupiter has a strong continuum emission at this frequency, stationary  
41 waves are generated within the instrument, causing ripples on the spectrum  
42 (Fig. 1). The subtraction of the ripples is the source of an uncertainty of 10%

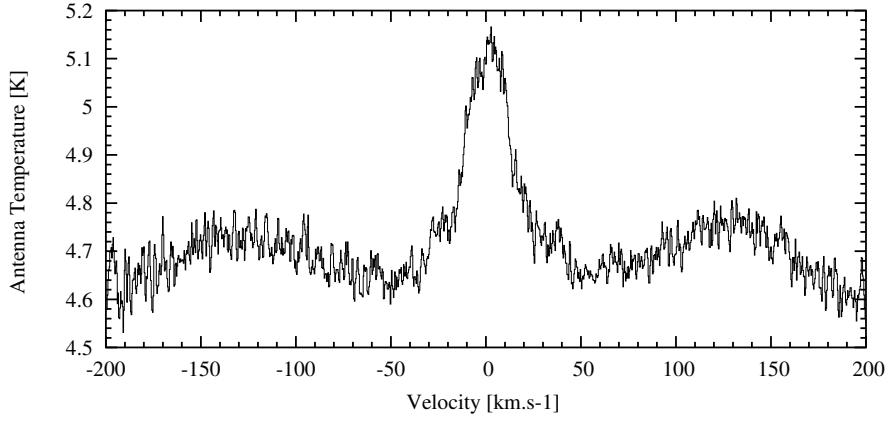


Fig. 1. Odin observations of Jupiter at the  $\text{H}_2\text{O}$  ( $1_{10}$ - $1_{01}$ ) line frequency on November 8, 2002. The observed antenna temperature is displayed as a function of velocity. The signal-to-noise ratio is 16.

43 on the line contrast and some uncertainty on the line wing shape.

44 As the beam size ( $3.3' \times 4.5'$  for SWAS and  $2.1'$  for Odin) is larger than the  
 45 planet size ( $\sim 35$ - $40''$ ), all the observed features correspond to the emission of  
 46 the whole planet. The line width is dominated by the smearing effect because  
 47 of limb equatorial velocity  $\sim 12.6 \text{ km.s}^{-1}$  of the planet (Bergin et al. 2000). As  
 48 no absolute calibration has been done for the Odin observations, all results are  
 49 discussed in terms of line-to-continuum ratios and the Odin/SWAS observed  
 50 continuum have been rescaled to the brightness temperature scale of our model  
 51 ( $T_B=128.6 \text{ K}$ ).

### 52 **3 Modeling**

53 We describe, in this section, details of our data analysis procedure that can  
 54 be summarized in the following way:

- 55 • A water vertical profile is simulated from a time-dependent 1D photochem-

56 ical model. The main parameters that affect this profile are the altitude  
57 and the magnitude of water deposition (in the case of a sporadic cometary  
58 origin), the magnitude of the water influx (in case of a steady interplanetary  
59 dust particle flux) and the eddy diffusion coefficient in the stratosphere.

- 60 • A radiative-transfer model computes a synthetic spectrum for each water  
61 vapor profile.
- 62 • Comparison of observational data and synthetic spectra enables to constrain  
63 parameters of the photochemical model.

### 64 3.1 Photochemical modeling

65 We used a time-dependent photochemical model, derived from the model de-  
66 veloped for Saturn by Ollivier et al. (2000) and which has been adapted to  
67 the case of the atmosphere of Jupiter. For each altitude and each chemical  
68 compound  $i$ , the code solves the continuity equation

$$69 \quad \frac{dn_i}{dt} = P_i - n_i L_i - \text{div}(\phi_i) \quad (1)$$

70 where  $n$  is the concentration,  $P$  the chemical production,  $L$  the chemical loss  
71 and  $\phi$  the vertical flux. This is a one-dimensional model since only the vertical  
72 transport is considered.

73 The model includes 46 oxygenated compounds and hydrocarbons and 593  
74 reactions (photolysis processes and chemical reactions). Condensation near  
75 the tropopause is also considered. The eddy diffusion coefficient profile we  
76 took comes from Moses et al. (2005). We chose their nominal eddy profile  
77 called “model C” (see Sect. 5). The influx rates of oxygenated compounds  
78 (proportion of H<sub>2</sub>O, CO<sub>2</sub> and CO) and H atoms were also taken from Moses

80 Moses et al. (2000) showed that an IDP source is more likely than a ring/satellite  
 81 source since there is a difference of  $\sim 2$  orders of magnitude in the estimated  
 82 fluxes. This is the reason why we chose to compare the results of two models:  
 83 an IDP source model and a low-IDP+SL9 source model. For the sake of sim-  
 84 plicity, the latter model will be called the SL9 model hereafter. The lack of  
 85 spatial resolution of the observations allowed us to use disk-averaged mixing  
 86 ratio vertical profiles for water, even if the SL9 impacts were all located in the  
 87 southern hemisphere. The only input parameter we had to fix to test the IDP  
 88 source hypothesis is the external flux of infalling water  $\Phi_{\text{H}_2\text{O}}^{\text{IDP}}$ . In order to test  
 89 the SL9 source hypothesis, we have built vertical profiles at the time of the  
 90 impacts (July 1994) and let them evolve with the photochemical model until  
 91 the time of the observations (September 1999, January 2001 for the SWAS  
 92 data and November 2002 for the Odin data). The initial water vertical profiles  
 93 have been built on the base of a low stationnary external flux and a sporadic  
 94 input, due to the comet. The low stationnary input flux is modeled via an IDP  
 95 model with a flux  $\Phi_{\text{H}_2\text{O}}^{\text{IDP}}=4\times 10^4 \text{ cm}^{-2}.\text{s}^{-1}$  (Lellouch et al. 2002). This value is  
 96 2 orders of magnitude lower than a pure IDP model (see Sect. 4). The spo-  
 97 radic input of water due to the impacts was modeled via two parameters: the  
 98 deposition pressure  $p_0$  and the initial mixing ratio  $q_0$  above the  $p_0$  level (see  
 99 Lellouch et al. 2002 for more details). For each computation, the value of  $q_0$   
 100 was set to a constant value as a function of altitude (above the  $p_0$  level).

101 Thus, we have two possibilities for the SL9 models. The first one consists of  
 102 fixing the value of  $p_0$  and adjusting the value of  $q_0$  with the data. In the second  
 103 case, we fix  $q_0$  and adjust  $p_0$ . Some constraints exist on both  $p_0$  and  $q_0$ . The  
 104 most reliable constraint is probably the fact that the deposition level that was

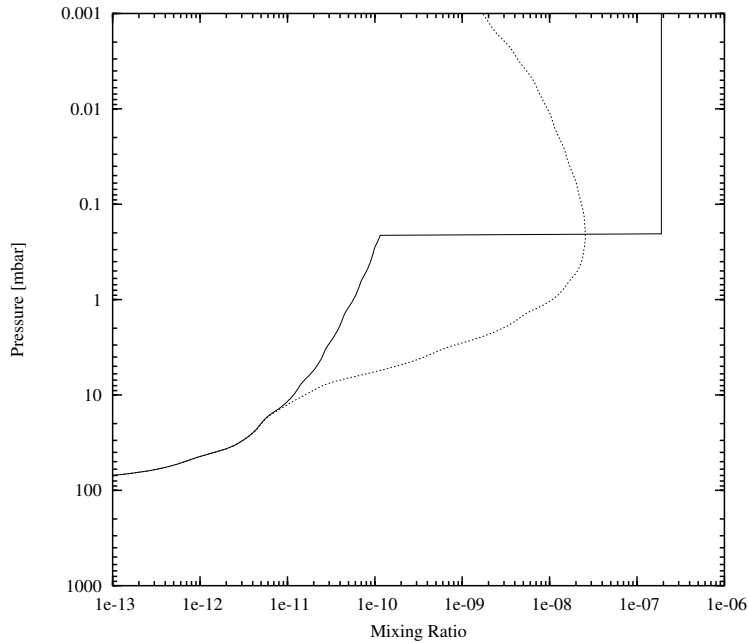


Fig. 2. Example of SL9 source vertical profiles of water at the time of the SL9 impacts (07/1994) in solid line and at the time of the Odin observations (11/2002) in dashed lines. The evolution of water abundance is computed by the photochemical model. The water vapor mixing ratio is displayed as a function of atmospheric pressure. Profiles correspond to a fixed value of  $p_0=0.2$  mbar, and an adjusted value of  $q_0=1.9\times 10^{-7}$ .

105 observed for CO during the SL9 impacts is  $0.2\pm 0.1$  mbar (Moreno 1998). From  
 106 CO and CS post-impact observations, Lellouch et al. (1995), Lellouch et al.  
 107 (1997) and Moreno et al. (2001) derived  $p_0$  levels of 0.3 mbar, 0.04-0.2 mbar  
 108 and 0.1 mbar (respectively). The other constraint lies on the observed column  
 109 density of water vapor. Lellouch et al. (2002) inferred that the  $\text{H}_2\text{O}/\text{CO}$  ratio  
 110 is equal to 0.07 in mass according to the entire ISO data set, thus fixing the  
 111  $\text{H}_2\text{O}$  column density to  $(2.0\pm 0.5)\times 10^{15}$   $\text{cm}^{-2}$ . Such a value lead to the derival  
 112 of a mixing ratio of water vapor of  $6 \times 10^{-8}$  above the deposition level. An  
 113 example of a SL9 model profile at the time of the impacts and at the time of  
 114 the Odin observations is shown on Fig. 2.



116 We modeled the observed submillimeter radiation with a line-by-line non-  
117 scattering radiative transfer model. We computed synthetic spectra of the  
118 H<sub>2</sub>O 557 GHz line. The program represents the approximate spherical geome-  
119 try of the planet so that planetary disk and limb contributions are taken into  
120 account. We assumed an uniform distribution of all other opacity sources and  
121 we adopted a mean thermal profile (see Fig. 3) of the atmosphere of Jupiter  
122 (Fouchet et al. 2000a) since our beam size is larger than the observed plan-  
123 etary disk. Continuum opacity is dominated by H<sub>2</sub>-He-CH<sub>4</sub> collision-induced  
124 absorption (Borysow et al. 1985, 1986 and 1988). Following Moreno (1998),  
125 the opacity due to the far wings of ammonia and phosphine lines was also  
126 included. We used the Fouchet et al. (2000b) ammonia and phosphine mixing  
127 ratio vertical profiles (see Fig. 4). Spectroscopic parameters for NH<sub>3</sub>, PH<sub>3</sub> and  
128 H<sub>2</sub>O were taken from Pickett et al. (1998). The line widths are determined by  
129 the collisional line widths for H<sub>2</sub> and He broadening. The broadening  $\gamma$  and  
130 temperature dependence exponent  $n$  values that we took for NH<sub>3</sub>, PH<sub>3</sub> and  
131 H<sub>2</sub>O are summarized in Table 1. All lines, except the NH<sub>3</sub> ones, were assumed  
132 to be Voigt-shaped. Following Moreno (1998), we took a modified Van Vleck  
133 and Weisskopf line profile for ammonia.

134 The rapid rotation of Jupiter (9.9 h) induces the smearing of the disk-averaged  
135 line on the spectrum, because of the Doppler shifts due to the gas rotation  
136 velocity (12.6 km.s<sup>-1</sup> at the eastern and western limbs). The way this effect  
137 is taken into account is described in Bergin et al. (2000).

138 We briefly come back to the use of disk-averaged vertical profiles of mixing

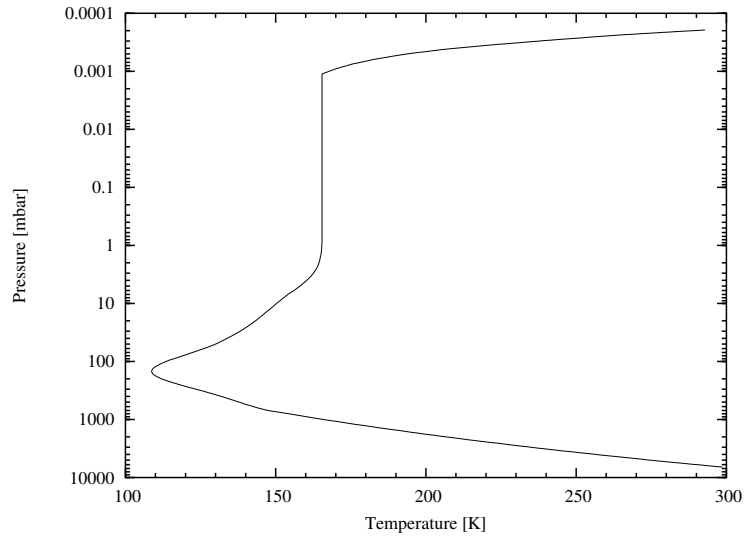


Fig. 3. Disk-averaged thermal profile of the atmosphere of Jupiter. The tropopause temperature is 109 K. The profile is isothermal ( $T=165.4$  K) between 1 mbar and  $10^{-3}$  mbar. Reference: Fouchet et al. (2000a).

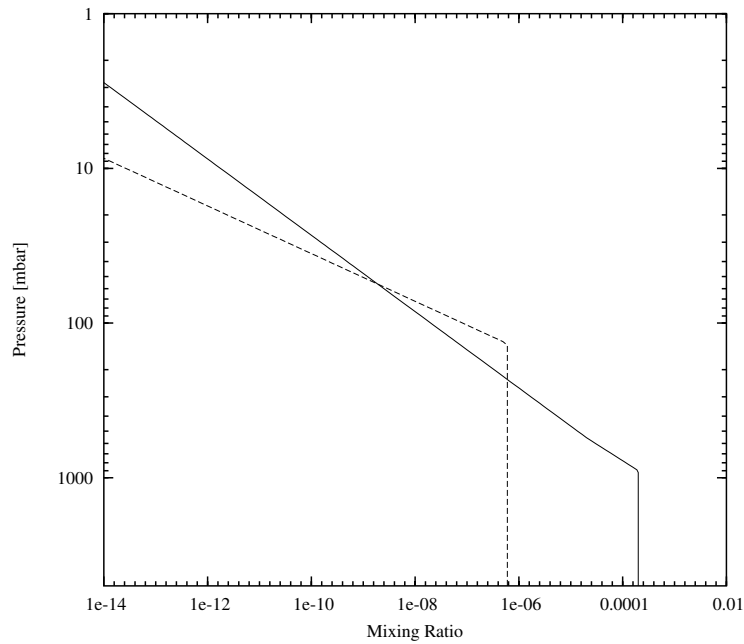


Fig. 4. Ammonia (solid line) and phosphine (long-dashed lines) mixing ratio vertical profiles as a function of pressure in Fouchet et al. (2000b).

139 ratio. The fact that the SL9 impacts were all located in the southern hemi-  
 140 sphere is not a limitation to our hypothesis. All the impacts occurred at the

$\gamma$	H <sub>2</sub>	He	Jupiter
NH <sub>3</sub>	0.069		0.069
PH <sub>3</sub> (2-1)	0.1064	0.0606	0.1001
H <sub>2</sub> O	0.0811	0.0228	0.0731
$n$	H <sub>2</sub>	He	Jupiter
NH <sub>3</sub>	0.67		0.67
PH <sub>3</sub>	0.73	0.30	0.67
H <sub>2</sub> O	0.9	0.50	0.85

Table 1

Collisional line width  $\gamma$  [ $cm^{-1}.atm^{-1}$ ] (at 300 K) and temperature dependance factor  $n$  for NH<sub>3</sub>, PH<sub>3</sub> and H<sub>2</sub>O with H<sub>2</sub> and He and for Jupiter (a blank space means that no data are available). References: Berge & Gulkis (1976) and Brown & Peterson (1994) for NH<sub>3</sub>, Levy et al. (1993,1994) for PH<sub>3</sub> and Dutta et al. (1993) for H<sub>2</sub>O.

141 latitude of 44°S. Longitudinal mixing proved to be efficient in the submillibar  
142 region. Indeed, HCN was observed at such pressure levels a few months after  
143 the comet impacts and the maps showed that it had already spread over sev-  
144 eral degrees in longitude (Bézarard et al. 1997). So, the deposits quickly formed  
145 a longitudinal belt after the impacts. Thus we have to take into account the  
146 background amount of water present in the stratosphere of Jupiter, which is  
147 due to the low IDP flux ( $\Phi_{H_2O}^{IDP}=4\times 10^4$  cm<sup>-2</sup>.s<sup>-1</sup>), and the SL9 input located  
148 at 44°S, which is modeled via the parameters  $p_0$  and  $q_0$ . By averaging those  
149 two kinds of vertical profiles over the surface of the planet, we obtain the  
150 kind of profile shown in Fig. 2 (see "hybrid model" in Lellouch et al. 2002),

151 where  $p_0$  is determined by the SL9 input and where  $q_0$  is multiplied by the  
152 ratio between the surface of the SL9 longitudinal belt and the total surface  
153 of the planet. Using this approach, the values of  $q_0$  we derive from the ob-  
154 servations are disk-averaged values. A disk-averaged water vertical profile is  
155 adapted since the beam size is greater than the planet size.

## 156 4 Results

157 The best-fit models have been determined with a  $\chi^2$  minimization process.  
158 All profiles and column density values are disk-averaged. One must note that  
159 an uncertainty of 5 K on the thermal profile would add an uncertainty of  
160  $0.4 \times 10^{15} \text{ cm}^{-2}$  on the water vapor column density,  $0.3 \times 10^{-7}$  on  $q_0$  (in the  
161 case of a SL9 origin) and  $0.6 \times 10^6 \text{ cm}^{-2} \cdot \text{s}^{-1}$  (in the case of an IDP origin).

### 162 4.1 SWAS data

163 The observed Rayleigh-Jeans temperature continuum of the 1999 and 2001 ob-  
164 servations are 126.4 K (Bergin et al. 2000) and 118.0 K (Lellouch et al. 2002)  
165 at  $-60 \text{ km} \cdot \text{s}^{-1}$  respectively. After rescaling the continuum value to the bright-  
166 ness temperature continuum of our model, it appears that only the SL9 models  
167 give satisfactory fits to both sets of data, either in the wings or in terms of line  
168 contrast. If we fit the line center, the IDP model with  $\Phi_{\text{H}_2\text{O}}^{\text{IDP}} = (3.4 \pm 0.5) \times 10^6$   
169  $\text{cm}^{-2} \cdot \text{s}^{-1}$  results in spectra which have too broad wings (see Fig. 5). It is not  
170 possible fit within the  $1\text{-}\sigma$  error bars the line center and the wings at the same  
171 time. The best-fit model for both SWAS datasets is obtained with a SL9 model  
172 with  $p_0 = 0.2 \text{ mbar}$  and  $q_0 = (1.8 \pm 0.5) \times 10^{-7}$  (see Figs. 5 and 6), leading to an

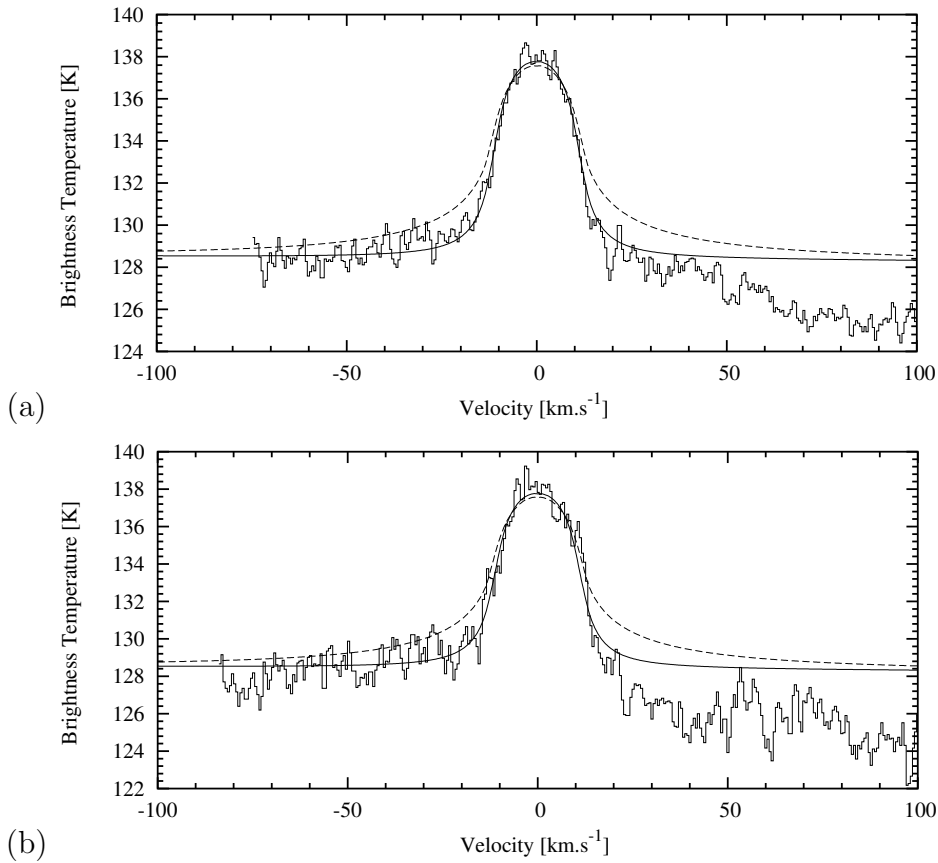


Fig. 5. Best-fit model to the (a) SWAS 1999 and (b) 2001 data obtained with a SL9 model with the initial parameters  $p_0=0.2$  mbar and  $q_0=1.8\times 10^{-7}$  (solid lines). The IDP models (long-dashed lines) correspond to infall fluxes of  $\Phi_{\text{H}_2\text{O}}^{\text{IDP}}=3.4\times 10^6$  cm<sup>-2</sup>.s<sup>-1</sup> for 1999 and 2001 respectively.

173 initial (in July 1994) column density of  $(3.5\pm 1.0)\times 10^{15}$  cm<sup>-2</sup>.

174 Nevertheless, the value of the continuum of both observations is quite uncer-  
 175 tain, mostly due to the broad spectral features. Shifting downward the value  
 176 of the continuum level within the error bar, it is possible to derive new values  
 177 of the IDP flux that permits us to obtain synthetic spectra that match the  
 178 SWAS data. For instance, if the continuum of the 1999 and 2001 observa-  
 179 tions are set to 125.4 K and 117.0 K (respectively) instead of 126.4 K and 118  
 180 K (respectively) and then rescaled to the brightness temperature continuum

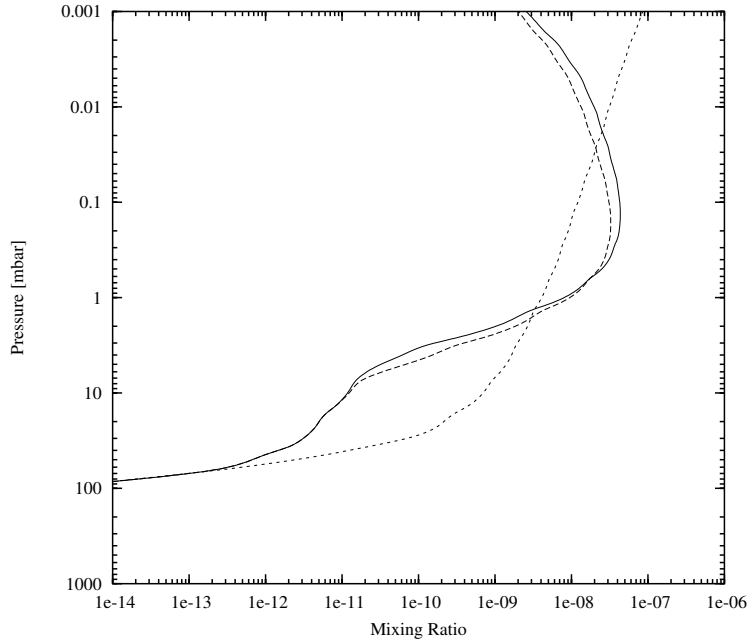


Fig. 6. Water mixing ratio vertical profiles as a function of pressure for a SL9 model with  $p_0=0.2$  mbar and  $q_0=1.8\times 10^{-7}$  at the time of the SWAS 1999 observations (solid line) and at the time of the SWAS 2001 observations (long-dashed lines) and for IDP models with a steady flux of water  $\Phi_{\text{H}_2\text{O}}^{\text{IDP}}=3.4\times 10^6$   $\text{cm}^{-2}.\text{s}^{-1}$  (short-dashed line). The column density of water is  $n_{\text{H}_2\text{O}}=3.5\times 10^{15}$   $\text{cm}^{-2}$  for the SL9 model at the time of the impacts and  $n_{\text{H}_2\text{O}}=2.6\times 10^{15}$   $\text{cm}^{-2}$  for the IDP model.

181 of our model ( $T_B=128.6$  K), then the fits of IDP models are far better (Fig.  
 182 7). The flux we derive is  $\Phi_{\text{H}_2\text{O}}^{\text{IDP}}=(3.7\pm 0.5)\times 10^6$   $\text{cm}^{-2}.\text{s}^{-1}$  and the correspond-  
 183 ing column density is  $(2.8\pm 0.4)\times 10^{15}$   $\text{cm}^{-2}$ . The synthetic spectrum is within  
 184 the  $1-\sigma$  error bars on the data over the  $[-80:+20]$   $\text{km}.\text{s}^{-1}$  range. Finally, the  
 185 IDP model cannot be ruled out at this stage, because of the uncertainty on  
 186 the continuum level of each observation, even if a  $\chi^2$  analysis shows that the  
 187 SL9 model gives a better match to the data than the IDP model. All the IDP  
 188 models that are considered for the SWAS data in what follows are models  
 189 with downward shifted continuum (to 125.4 K and 117.0 K, for 1999 and 2001  
 190 respectively).

191 The SL9 model where  $q_0$  is fixed to  $6 \times 10^{-8}$  also gives a good fit for  $p_0 = (0.45 \pm$   
 192  $0.09)$  mbar (see Fig. 8). Here, the error bar on the  $p_0$  value is not due to the  
 193  $1-\sigma$  level of the spectrum. Indeed, the synthetic spectra with either  $p_0 = 0.37$   
 194 mbar or  $p_0 = 0.54$  mbar are outside the  $1-\sigma$  level of the spectrum. This error  
 195 bar is due to the fact that the integration step of the photochemical model  
 196 is 5 km. This results in 0.09 mbar steps in the 0.2-0.6 mbar region. Taking  
 197  $p_0 = 0.45$  mbar and  $q_0 = 6 \times 10^{-8}$ , the column density of water is  $(2.6 \pm 0.6) \times 10^{15}$   
 198  $\text{cm}^{-2}$  at the time of the impacts.

#### 199 4.2 *Odin data*

200 After removing the ripple pattern, the line shows some asymmetry in the line  
 201 wings. This, as well as the noise level, is a limitation in the determination  
 202 of the best-fit model. Testing the IDP fluxes leads us to retrieve of a lower  
 203 flux than the flux retrieved from the SWAS data. Indeed, the  $\chi^2$  minimum is  
 204 obtained for a flux value of  $\Phi_{\text{H}_2\text{O}}^{\text{IDP}} = (3.4 \pm 0.5) \times 10^6 \text{ cm}^{-2} \cdot \text{s}^{-1}$  (see Fig. 9). This  
 205 result is compatible with the SWAS initial results (before shifting downward  
 206 the Rayleigh-Jeans temperature continuum). If we try to fit the line with an  
 207 averaged best-fit model to the SWAS/Odin data ( $\Phi_{\text{H}_2\text{O}}^{\text{IDP}} = 3.6 \times 10^6 \text{ cm}^{-2} \cdot \text{s}^{-1}$ ),  
 208 then the line center is better reproduced (see Fig. 9). Nevertheless, such a  
 209 modeling results in broader wings, but they still are within the  $1-\sigma$  error bars.

210 As for the SL9 model, restraining the bulk of water above an initial pressure  
 211 level of 0.2 mbar, results in narrower lines than the IDP model. The line  
 212 center as well as the wings are well reproduced with the synthetic spectra.  
 213 When fixing  $p_0$  to 0.2 mbar, the optimum water mixing ratio above this level  
 214 is  $q_0 = 2.0 \times 10^{-7}$ . The uncertainty is  $0.5 \times 10^{-7}$ . When fixing  $q_0$  to  $6.0 \times 10^{-8}$

215 (Lellouch et al. 2002),  $p_0$  is found to be  $(0.54\pm 0.09)$  mbar (see Fig. 10). The  
216 latter model implies a column density of  $(3.2\pm 0.6)\times 10^{15}$   $\text{cm}^{-2}$  at the time of  
217 the comet impacts.

## 218 5 Discussion

219 The best-fit model parameters for each observation, as derived from  $\chi^2$  mini-  
220 mization, are summarized in Table 2. From this set of parameters, we derived  
221 averaged values. For each model (IDP, SL9 with  $q_0$  fixed and SL9 with  $p_0$   
222 fixed), the value obtained is affected a weight related to the signal-to-noise  
223 ratio of the observation. Doing this way, we obtained the averaged values used  
224 in Fig. 11.

225 First of all, when considering the SL9 source hypothesis and fixing the value  
226 of  $q_0$  at  $6\times 10^{-8}$ , we derive a deposition pressure level  $p_0$  in the range of 0.45-  
227 0.54 mbar. The column density we derived is consistent with the value of  
228 Lellouch et al. (2002). However, even if our model does not provide a more  
229 precise value of  $p_0$ , the range of the values we derive is outside the ranges  
230 derived by Lellouch et al. (1997) and Moreno (1998) from CO observations at  
231 millimeter wavelengths at the time of the impacts, which are 0.04-0.2 mbar and  
232  $0.2\pm 0.1$  mbar (respectively). Therefore, we regard this possibility as unlikely  
233 with regard to both SWAS and Odin data.

234 So, the models we have to compare are the IDP model and the SL9 model with  
235  $p_0=0.2$  mbar. We derived an external flux of water, originating from an IDP  
236 source, of  $\Phi_{\text{H}_2\text{O}}^{\text{IDP}}=(3.6\pm 0.5)\times 10^6$   $\text{cm}^{-2}\cdot\text{s}^{-1}$ . This value is greater than the one  
237 derived by Bergin et al. (2000) by a factor of less than 2. From their physical



238 model, which only included vertical transport (no chemical or photochemical  
239 processes), the authors derived a deposition flux of  $2.0 \times 10^6 \text{ cm}^{-2} \cdot \text{s}^{-1}$ . To ob-  
240 tain a narrower line from their model and thus to obtain their best-fit model,  
241 they increased the mixing ratio over pressure slope ( $-\text{d}(\log q)/\text{d}(\log p)$ ) of their  
242 physical profile from 0.8 to 1.3. Nevertheless, as noted by the authors, chang-  
243 ing the slope could not simulate precisely the effects of photolysis, chemical  
244 reactions and the non-linearity of the interactions between these processes as  
245 well as vertical transport and condensation. Taking photolysis and chemical  
246 losses into account, they would probably have obtained a higher value for the  
247 flux consistent with our result.

248 With a SL9 model, we obtain  $q_0 = (1.9 \pm 0.5) \times 10^{-7}$  when fixing  $p_0 = 0.2$  mbar.  
249 Lellouch et al. (2002) derived a column density of  $(2.0 \pm 0.5) \times 10^{15} \text{ cm}^{-2}$  at the  
250 time of the ISO observations. The column density we derived is  $(3.7 \pm 1.0) \times 10^{15}$   
251  $\text{cm}^{-2}$  at the time of the impacts. This value is greater than the ISO value,  
252 but by taking photolysis, chemical reactions, vertical transport and conden-  
253 sation, this value decreases down to  $(3.1 \pm 0.8) \times 10^{15} \text{ cm}^{-2}$  at the time of ISO  
254 observations. This value is still above the Lellouch et al. (2002) value, but  
255 there is a small overlap on the ranges of values. Moreover, considering an un-  
256 certainty of 5 K on the thermal profile ends up in an additional uncertainty  
257 of  $0.4 \times 10^{15} \text{ cm}^{-2}$  on the column abundance. So, these values could well be  
258 consistent and an intermediate value of column density should be compatible  
259 with all inferred values. As the water vapor vertical profile of Lellouch et al.  
260 (2002) was computed from a vertical transport model, the ISO data should be  
261 re-analysed with a more complete photochemical model. This work still has  
262 to be done and its results could be directly comparable to ours.

263 The SL9 model quoted above better reproduces the line contrast as well as the

SWAS 1999 and 2001			
Model	$\Phi_{\text{H}_2\text{O}}^{\text{IDP}} [\text{cm}^{-2}.\text{s}^{-1}]$	$p_0$ [mbar]	$q_0$
IDP	$(3.7\pm 0.5)\times 10^6$	-	-
SL9 ( $q_0$ fixed)	$4.0\times 10^4$	$(0.45\pm 0.09)$	$6\times 10^{-8}$
SL9 ( $p_0$ fixed)	$4.0\times 10^4$	0.2	$(1.8\pm 0.5)\times 10^{-7}$
Odin 2002			
Model	$\Phi_{\text{H}_2\text{O}}^{\text{IDP}} [\text{cm}^{-2}.\text{s}^{-1}]$	$p_0$ [mbar]	$q_0$
IDP	$(3.4\pm 0.5)\times 10^6$	-	-
SL9 ( $q_0$ fixed)	$4.0\times 10^4$	$(0.54\pm 0.09)$	$6\times 10^{-8}$
SL9 ( $p_0$ fixed)	$4.0\times 10^4$	0.2	$(2.0\pm 0.5)\times 10^{-7}$

Table 2

Best-fit model parameters for each set of data and each model, from which the averaged best-fit value are derived (see text).

264 line wings than the IDP model (see Fig. 11). A  $\chi^2$  analysis clearly indicates  
265 that the SL9 model gives better fits to the data. However, all the IDP synthetic  
266 spectra are within the  $1\text{-}\sigma$  error bars on all observations. So, this model cannot  
267 be ruled out at this stage.

268 If the observed water would come from the SL9 comet, then the non-steady  
269 state created by the deposition of the cometary material above the  $p_0$  level  
270 in our model should evolve towards a steady state where the only observable  
271 source of water would be the low IDP flux ( $4\times 10^4 \text{ cm}^{-2}.\text{s}^{-1}$  in our model).  
272 From our computations, such a state is reached  $\sim 400$  years after the im-

273 pacts. As a result, the downward diffusion of water as well as the photochem-  
274 ical/chemical losses effects would first desaturate the line. Thus, the line con-  
275 trast should first increase with time (see Fig. 12). Our photochemical model  
276 predicts that the line center temperature of the line should increase by 0.76 K  
277 from 1999 to 2007. Taking the noise level of the SWAS 1999 observations into  
278 account, our model predicts that this effect could only be observed in 2007 by  
279 reaching a signal-to-noise ratio of 50 with the Odin telescope. Afterwards, the  
280 amount of water decreasing more and more with time at submillibar pressures,  
281 the line should become fainter and broader and should tend towards the line  
282 that would be due to the low IDP flux only (see Fig. 12). This change should  
283 be observable with Herschel-HIFI.

284 One must not forget that the shape of the water vertical profile computed  
285 with a photochemical model highly depends on the vertical eddy diffusion  
286 coefficient profile  $K(z)$ . Due to strong uncertainties in the chemical scheme,  
287 each photochemical model derives, from comparison with observational data,  
288 a new value of  $K(z)$  that can differ by about one order of magnitude at some  
289 altitudes (see Dobrijevic & Parisot 1998, Dobrijevic et al. 2003 and Hébrard  
290 et al. 2007 for a detailed discussion on this point). For instance, as shown on  
291 Fig. 7 of Moses et al. (2005), many different  $K(z)$  profiles have been inferred  
292 from past observations. At the submillibar pressure range,  $K(z) \simeq 5 \times 10^4$   
293  $\text{cm}^{-2} \cdot \text{s}^{-1}$  within a factor of 2 (Moreno et al. 2003). According to the Moses  
294 et al. (2005) model C value used in this work,  $K(z)$  is equal to  $7.8 \times 10^4$   
295  $\text{cm}^{-2} \cdot \text{s}^{-1}$ . At pressures between 0.1 mbar and 100 mbar (tropopause level),  
296 Gladstone et al. (1996) found values of  $K(z)$  higher by a factor of  $\sim 3$ . So  
297 we have to consider the fact that another choice in the  $K(z)$  profile could  
298 change our results. In the lower stratosphere, our adopted  $K(z)$  profile gives

299 a lower limit to  $K(z)$  values (see Fig. 7 in Moses et al. 2005). By taking the  
300 Gladstone et al.(1996)  $K(z)$  profile, we would obtain an eddy mixing in the  
301 lower stratosphere more efficient than in our study and it would result in more  
302 water above the condensation level. The direct impact on the spectra of such  
303 a change in the  $K(z)$  profile would be a broadening of the wings. Thus, the  
304 IDP origin synthetic spectra would be out of the  $1-\sigma$  error bars of the SWAS  
305 and Odin observations. Finally, taking Moses et al. (2005) model C as a  $K(z)$   
306 profile is a conservative way of analysing the observed lines with regard to the  
307 implications noted above.

## 308 6 Conclusion

309 In this paper, we have shown that the high signal-to-noise ratio observations  
310 of water vapor in the stratosphere of Jupiter, carried out with SWAS and the  
311 Odin telescope between 1999 and 2002, favor a SL9 origin for water. Indeed,  
312 all observations are better fitted when the bulk of water is restricted to sub-  
313 millibar pressures. In our disk-averaged and simplified deposition model of  
314 the SL9 water, we derived a water mixing ratio of  $1.9 \times 10^{-7}$  above an initial  
315 pressure deposition level of 0.2 mbar. In this model, a low IDP flux of  $4 \times 10^4$   
316  $\text{cm}^{-2} \cdot \text{s}^{-1}$  was also taken into account. This suggests a localised input of water,  
317 in terms of altitude, which is contradictory with a steady state resulting from  
318 an IDP permanent flux. Nevertheless, all synthetic spectra obtained from an  
319 IDP flux of  $\Phi_{\text{H}_2\text{O}}^{\text{IDP}} = (3.6 \pm 0.5) \times 10^6 \text{ cm}^{-2} \cdot \text{s}^{-1}$  give fits that are within the  $1-\sigma$  er-  
320 ror bars of the observations, but the  $\chi^2$  value is greater than the one computed  
321 from the SL9 model. In view of these results, the ISO data of 1997 should be  
322 re-analysed using the model developped in this work.

323 Further observations, reaching a higher signal-to-noise ratio are needed to  
324 state on the origin of water vapor in the stratosphere of Jupiter, even if the  
325 SL9 origin is favored by both SWAS and Odin observations. The analysis of  
326 the latest Odin observations (August 2007) is underway. Moreover, Herschel  
327 observations with the HIFI instrument (500 GHz - 2000 GHz) should allow ob-  
328 taining a signal-to-noise ratio with a comparable spectral resolution in reason-  
329 able times. Such a high signal-to-noise ratio would enable us to better resolve  
330 the line wing shape in order to discriminate between both origins. Moreover,  
331 a temporal variability of the line could be brought to light. Such a variability  
332 should not be expected with an IDP origin. Indeed, Moses et al. (2000a) sug-  
333 gested that the production of the IDP is dominated by short-period comets.  
334 Selsis et al. (2004) showed that 48 short-period ( $\sim 5$ -10 year periods) comets  
335 approach Jupiter's orbit at less than the Roche lobe radius of the planet. So,  
336 the IDP flux on Jupiter should be steady. Finally, using HIFI at the highest  
337 frequencies would result in a sufficient spatial resolution to carry out maps of  
338 Jupiter at water vapor frequencies. A latitudinal inhomogeneous distribution  
339 of water, with an increase of its amount in the southern hemisphere would be  
340 a strong signature of a SL9 impact origin and could provide information on  
341 the horizontal diffusion at the submillibar level.

## 342 **References**

- 343 [1] Berge, G. L., Gulkis, S., 1976, In "Jupiter, studies of the interior, atmo-  
344 sphere, magnetosphere and satellites", ed. T. Gehrels, 621-692
- 345 [2] Bergin, E. A., Lellouch, E., Harwit, M., Gurwell, M. A., Melnick, G. J.,  
346 Ashby, M. L. N., Chin, G., Erickson, N. R., Goldsmith, P. F., Howe, J. E.,  
347 Kleiner, S. C., Koch, D. G., Neufeld, D. A., Patten, B. M., Plume, R.,

- 348 Schneider, R., Snell, R. L., Stauffer, J. R., Tolls, V., Wang, Z., Winnewisser,  
349 G., Zhang, Y. F., 2000, *The Astrophysical Journal*, 539, L147-L150
- 350 [3] Bézard, B., Griffith, C. A., Kelly, D. M., Lacy, J. H., Greathouse, T.,  
351 Orton, G., 1997, *Icarus*, 125, 94-120
- 352 [4] Borysow, J., Trafton, L., Frommhold, L., Birnbaum, G., 1985, *The Astro-*  
353 *physical Journal*, 296, 644-654
- 354 [5] Borysow, A., Frommhold, L., 1986, *The Astrophysical Journal*, 304, 849-  
355 865
- 356 [6] Borysow, J., Frommhold, L., Birnbaum, G., 1988, *The Astrophysical Jour-*  
357 *nal*, 326, 509-515
- 358 [32] Brown, L. R., Peterson, D. B., 1994, *Journal of Molecular Spectroscopy*,  
359 168, 593-606
- 360 [8] Dobrijevic, M., Parisot, J.-P., 1998, *Planetary and Space Science*, 46, 491-  
361 505
- 362 [9] Dobrijevic, M., Ollivier, J.-L., Billebaud, F., Parisot, J.-P., 2003, *Astron-*  
363 *omy and Astrophysics*, 398, 335-344
- 364 [10] Dutta, J. M., Jones, C. R., Goyette, T. M., De Lucia, F. C., 1993 *Icarus*,  
365 102, 232-239
- 366 [11] Feuchtgruber, H., Lellouch, E., de Graauw, T., Bézard, B., Encrenaz, T.,  
367 Griffin, M., 1997, *Nature*, 389, 159-162
- 368 [12] Feuchtgruber, H., Lellouch, E., Encrenaz, T., Bézard, B., Coustenis, A.,  
369 Drossart, P., Salama, A., de Graauw, T., Davis, G. R., 1999, *The Universe*  
370 *as Seen by ISO*, Eds., P. Cox & M.F. Kessler, ESA-SP, 427, 133
- 371 [13] Fouchet, T., Lellouch, E., Bézard, B., Feuchtgruber, H., Drossart, P.,  
372 Encrenaz, T., 2000a, *Astronomy and Astrophysics*, 355, L13-L17
- 373 [14] Fouchet, T., Lellouch, E., Bézard, B., Encrenaz, T., Drossart, P., Feucht-

- 374 gruber, H., de Graauw, T., 2000b, *Icarus*, 143, 223-243
- 375 [15] Gladstone, G.R., Allen, M., Yung, Y. L., 1996, *Icarus*, 119, 1-52
- 376 [16] Hébrard, E., Dobrijevic, M., Bénilan, Y., Raulin, F., 2007, *Planetary and*  
377 *Space Science*, 55, 1470-1489
- 378 [17] Lellouch, E., Paubert, G., Moreno, R., Festou, M. C., Bézard, B.,  
379 Bockelée-Morvan, D., Colom, P., Crovisier, J., Encrenaz, T., Gautier, D.,  
380 Marten, A., Despois, D., Strobel, D. F., Sievers, A., 1995, *Nature*, 373,  
381 592-595
- 382 [18] Lellouch, E., Bézard, B., Moreno, R., Bockelée-Morvan, D., Colom, P.,  
383 Crovisier, J., Festou, M., Gautier, D., Marten, A., Paubert, G., 1997, *Plan-*  
384 *etary and Space Science*, 45, 1203-1212
- 385 [19] Lellouch, E., 1999, *The Universe as Seen by ISO*, Eds., P. Cox & M. F.  
386 Kessler, ESA-SP, 427, 125
- 387 [20] Lellouch, E., Bézard, B., Moses, J. I., Davis, G. R., Drossart, P., Feucht-  
388 gruber, H., Bergin, E. A., Moreno, R., Encrenaz, T., 2002, *Icarus*, 159,  
389 112-131
- 390 [21] Levy, A., Lacome, N., Tarrago, G., 1993, *Journal of Molecular Spec-*  
391 *troscopy*, 157, 172-181
- 392 [22] Levy, A., Lacome, N., Tarrago, G., 1994, *Journal of Molecular Spec-*  
393 *troscopy*, 166, 20-31
- 394 [23] Moreno, R., 1998, PhD Thesis, Université Paris VI
- 395 [24] Moreno, R., Marten, A., Biraud, Y., Bézard, B., Lellouch, E., Paubert,  
396 G., Wild, W., 2001, *Planetary and Space Science*, 49, 473-486
- 397 [25] Moreno, R., Marten, A., Matthews, H. E., Biraud, Y., 2003, *Planetary*  
398 *and Space Science*, 51, 591-611
- 399 [26] Moses, J. I., Bézard, B., Lellouch, E., Gladstone, G. R., Feuchtgruber,

- 400 H., Allen, M., 2000a, *Icarus*, 143, 244-298
- 401 [27] Moses, J. I., Lellouch, E., Bézard, B., Gladstone, G. R., Feuchtgruber,  
402 H., Allen, M., 2000b, *Icarus*, 145, 166-202
- 403 [28] Moses, J. I., Fouchet, T., Bézard, B., Gladstone, G. R., Lellouch, E.,  
404 Feuchtgruber, H., 2005, *Journal of Geophysical Research*, 110, E08001
- 405 [29] Olberg, M., Frisk, U., Lecacheux, A., Olofsson, A. O., Baron, P., Bergman,  
406 P., Florin, G., Hjalmarson, Å, Larsson, B., Murtagh, D., Olofsson, G., Pa-  
407 gani, L., Sandqvist, Aa., Teyssier, D., Torchinsky, S. A., Volk, K., 2003,  
408 *Astronomy and Astrophysics*, 402, L35-L38
- 409 [30] Ollivier, J.-L., Dobrijevic, M., & Parisot, J.-P., 2000, *Planetary and Space*  
410 *Science*, 48, 699
- 411 [31] Pickett, H. M., Poynter, R. L., Cohen, E. A., Delitsky, M. L., Pearson,  
412 J. C., Muller, H. S. P., 1998, *Journal of Quantitative Spectroscopy and*  
413 *Radiative Transfer*, 60, 883
- 414 [32] Selsis, F., Brillet, J., Rapaport, M., 2004, *Astronomy and Astrophysics*,  
415 416, 783-789



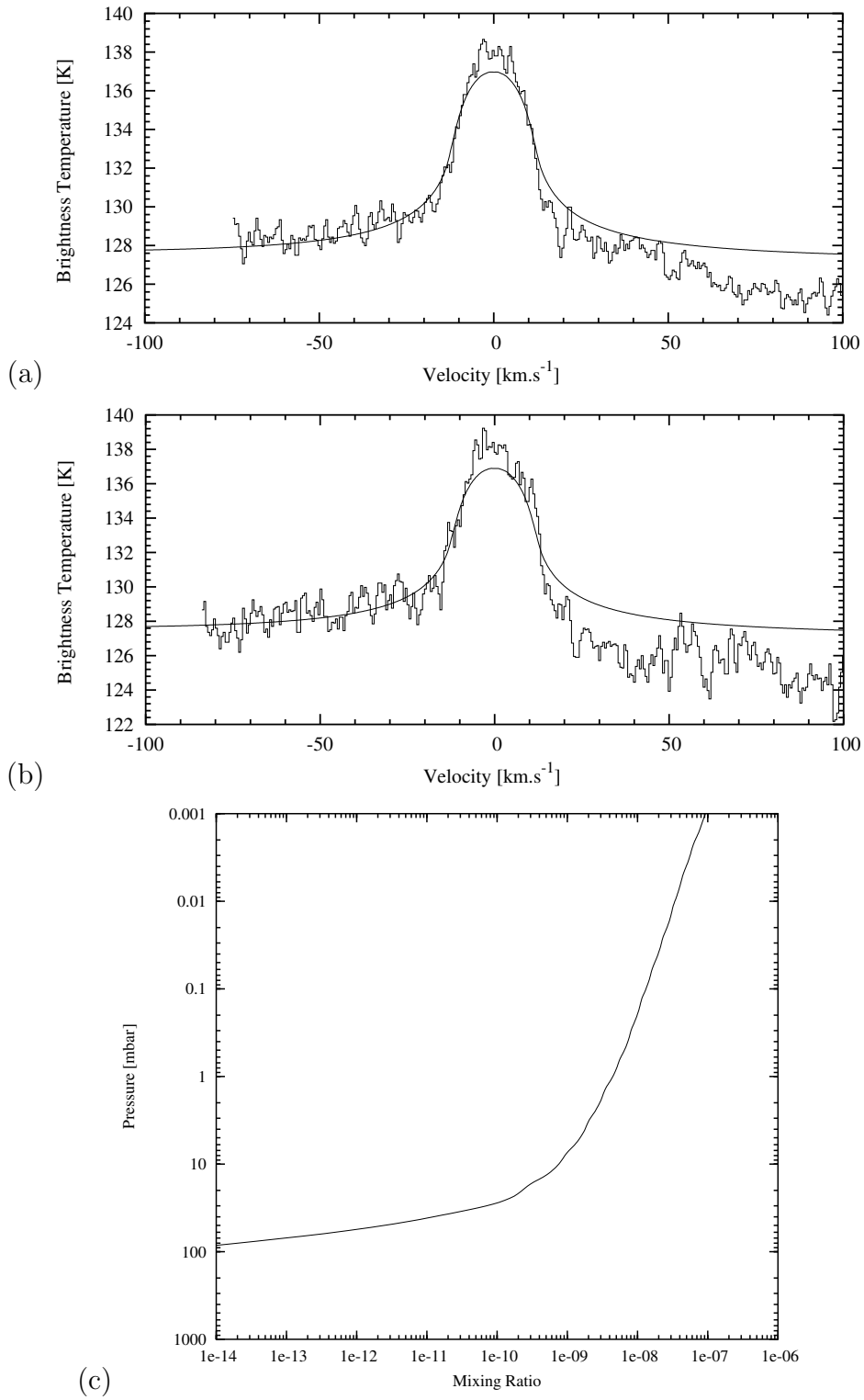


Fig. 7. Brightness temperature spectra as observed by SWAS (a) in 1999 and (b) in 2001. Both spectrum continuum have been rescaled so as to obtain a better fit of the line wings with an IDP model. (c): water mixing ratio vertical profile as a function of pressure resulting from the observed flux of  $\Phi_{\text{H}_2\text{O}}^{\text{IDP}} = 3.7 \times 10^6 \text{ cm}^{-2} \cdot \text{s}^{-1}$ .

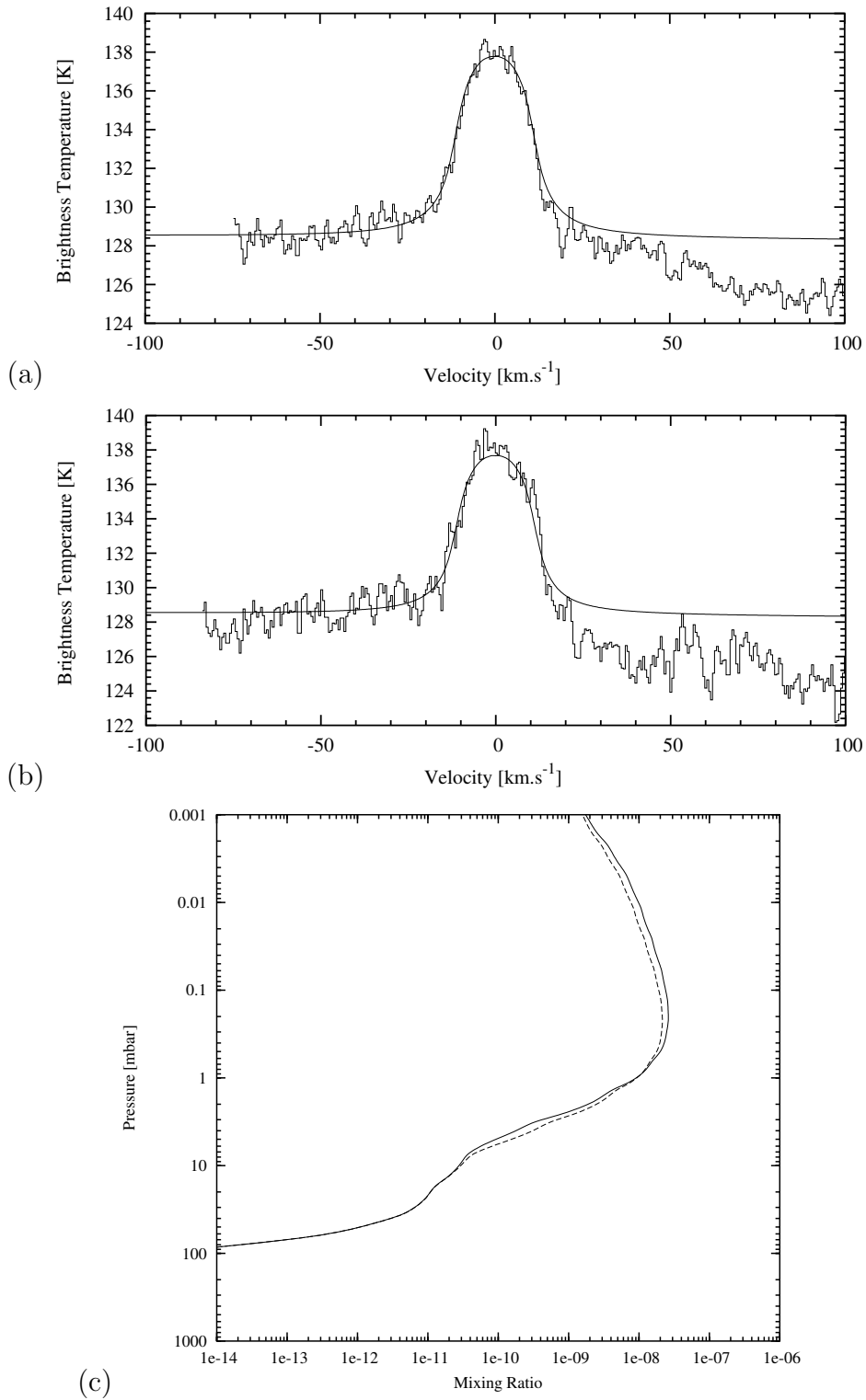


Fig. 8. SL9 model results compared to the (a) SWAS 1999 and (b) SWAS 2001 observed spectra, when fixing  $q_0=6.0\times 10^{-8}$ . The derived initial deposition pressure level  $p_0$  is 0.45 mbar. (c): corresponding water mixing ratio vertical profiles at the time of the observations (solid line for 1999 and long-dashed lines for 2001).

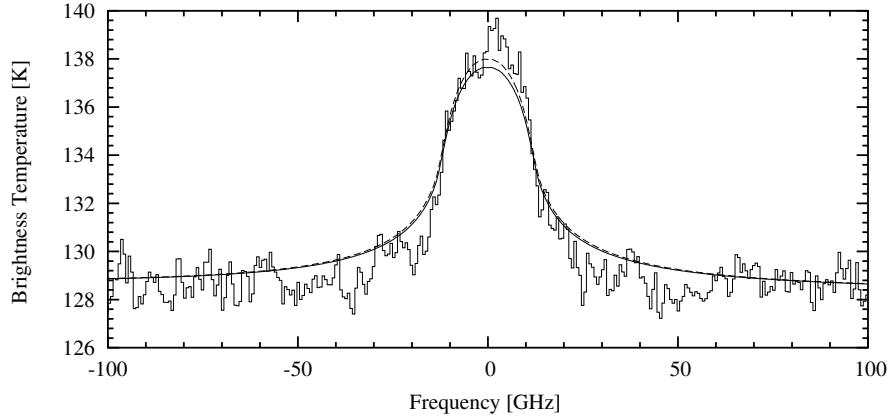


Fig. 9. Odin 2002 data modeled with IDP models. The solid line corresponds to a flux of  $\Phi_{\text{H}_2\text{O}}^{\text{IDP}} = 3.4 \times 10^6 \text{ cm}^{-2} \cdot \text{s}^{-1}$  ( $\chi^2$  minimum value). The long-dashed lines correspond to the overall (SWAS and Odin data) best-fit model ( $\Phi_{\text{H}_2\text{O}}^{\text{IDP}} = 3.6 \times 10^6 \text{ cm}^{-2} \cdot \text{s}^{-1}$ ).

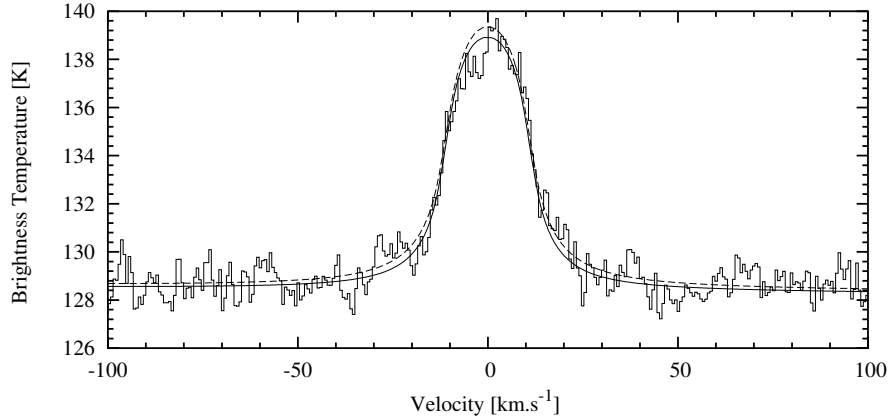


Fig. 10. Odin 2002 data modeled with SL9 models. When  $p_0$  is fixed to 0.2 mbar, the derived  $q_0$  value is  $2.0 \times 10^{-7}$  (solid line) whereas when fixing  $q_0$  to  $6.0 \times 10^{-8}$ , the derived  $p_0$  pressure level is 0.54 mbar (long-dashed lines).

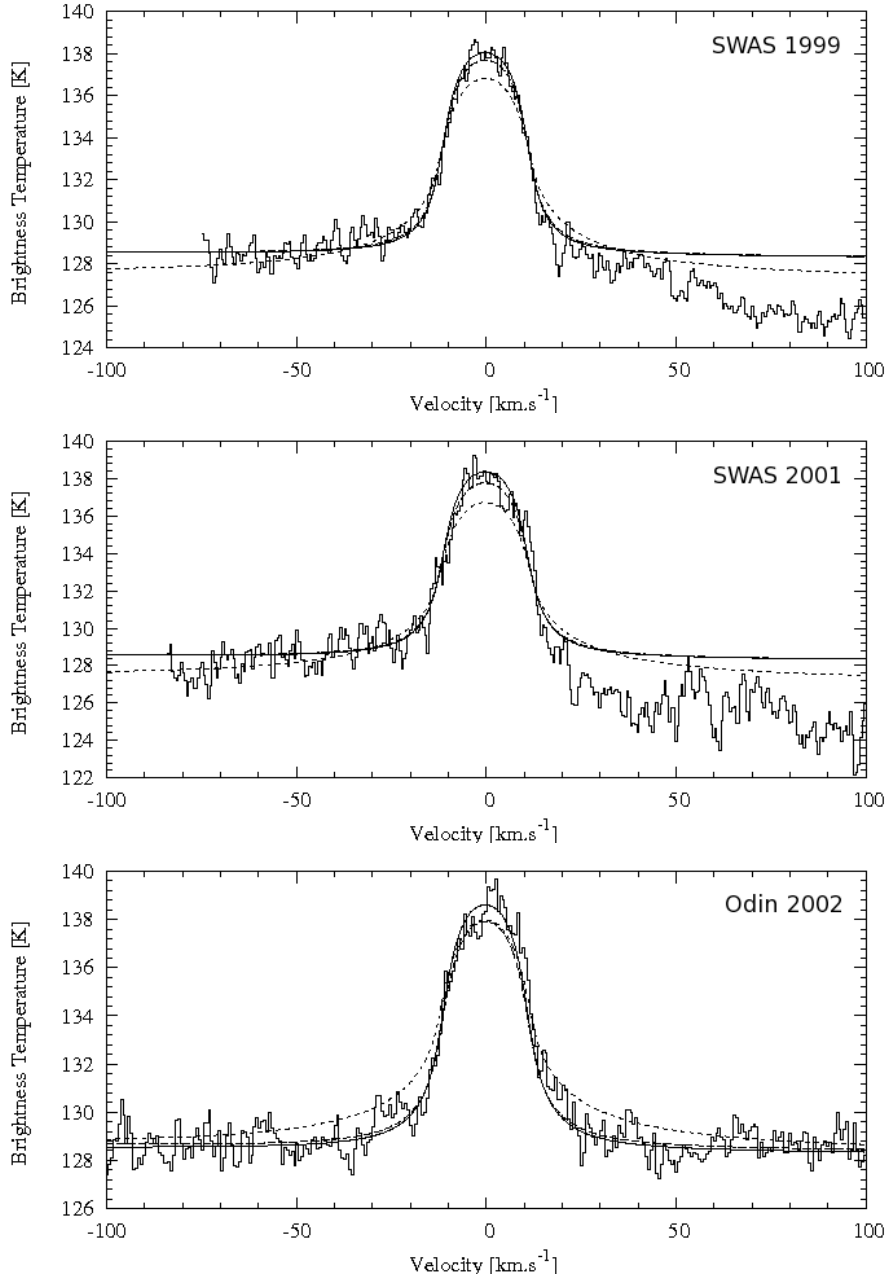


Fig. 11. Overall best-fit models for the SWAS 1999 and 2001 and Odin 2002 observations. Solid lines: SL9 model with  $p_0=0.2$  mbar (fixed) and  $q_0=1.9\times 10^{-7}$ ; long-dashed lines: SL9 model with  $p_0=0.45$  mbar and  $q_0=6\times 10^{-8}$  (fixed); short-dashed lines: IDP model with a steady infall flux of water  $\Phi_{\text{H}_2\text{O}}^{\text{IDP}}=3.6\times 10^6 \text{ cm}^{-2}.\text{s}^{-1}$ . The overall best-fit parameter have been obtained from Table 2 and by taking the signal-to-noise ratio of each observation into account. Doing this way, the SWAS 1999 observations have a lower impact on the results than the SWAS 2001 and Odin 2002 observations.

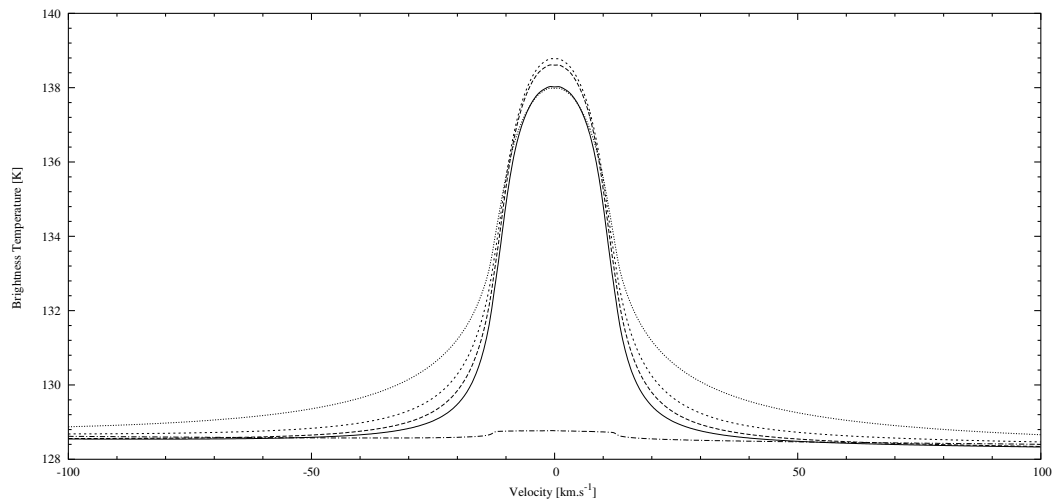


Fig. 12. Evolution of the line shape with time, in the case of a SL9 origin. Vertical distribution of water has been computed with our photochemical model at various dates. Parameters  $p_0$  and  $q_0$  have been set to 0.2 mbar and  $1.9 \times 10^{-7}$  respectively. The spectrum is plotted at the time of SWAS 1999 observations (solid line), Odin 2002 observations (long-dashed lines), in 2007 as observed with the Odin telescope (short-dashed lines). Once all the water deposited by SL9 will be removed by photochemistry, transport and condensation, the remaining water will only be due to the low IDP flux ( $\Phi_{\text{H}_2\text{O}}^{\text{IDP}} = 4 \times 10^4 \text{ cm}^{-2} \cdot \text{s}^{-1}$ ). The dashed-dotted lines represent the line due to this flux, as it would be observed by Odin. The line resulting from an IDP model ( $\Phi_{\text{H}_2\text{O}}^{\text{IDP}} = 3.6 \times 10^6 \text{ cm}^{-2} \cdot \text{s}^{-1}$ ) is plotted for comparison in dotted lines.